Engineering Solid Mechanics 10 (2022) 129-138

Contents lists available at GrowingScience

Engineering Solid Mechanics

homepage: www.GrowingScience.com/esm

Comparison between structural configurations designed by steel shear wall, moment resistant frame and X shape bracing systems

Mohammad Gholami[a*], Mehrdad Dorj[a], Peyman Beiranvand[b], Pegah Jafari Haghighatpour[c] and Aref Azamigilan[d]

[a]*Department of Civil Engineering, Yasouj University, Yasouj, Iran*
[b]*Department of Civil Engineering, Lorestan University, Khorramabad, Iran*
[c]*Welding and Joining Research Center, School of Industrial Engineering, Iran University of Science and Technology (IUST), Narmak, 16846-13114, Tehran, Iran*
[d]*Department of Mechanical Engineering, Barcelona East School of Engineering, Technical University of Catalonia Barcelona Tech, Barcelona, Spain*

ARTICLEINFO

Article history:
Received 2 December 2021
Accepted 14 February 2022
Available online
14 February 2022

Keywords:
CFT column
Steel shear wall
Non-linear time-history analysis
Structural analyses
SAP2000
ABAQUS modeling

ABSTRACT

Nowadays, in order to increase construction of tall structures, the importance of choosing optimum systems, with a huge energy absorption capacity against wind and earthquake loads, has been widely considered. Since four decades ago, steel shear walls had been used as a stiff and high performance lateral system. This study is about the effect of concrete filled steel tubes (CFT) columns as vertical boundary elements of steel shear wall on seismic behavior of steel structures. Due to do this, three 10-storey steel structures, with similar plans and lateral load career systems of steel shear wall, coinciding X-bracing, and moderate steel frame were analyzed by means of non-linear, time-history method through SAP2000 software, and the results of roof displacement of them were compared with each other. Also after validating a two-storey, single-span frame sample with steel shear walls and CFT columns, 3 single-storey structures were analyzed by means of hysteresis and pushover, through ABAQUS software. The results of this study showed that a shear wall system presents suitable stiffness, resistance and ductility in comparison with other lateral bearing systems.

1. Introduction

Design of seismic-resistant structures is one of the major concerning fields of civil engineers. Thus, implementation of novel technologies such as composite concrete-filled columns seems to be critical to improve the seismic behavior of structures. Nowadays, these columns are widely used in the construction industry because of their high resistance and seismic performance. The steel constrains the concrete inside the column and significantly raises the resistance and stiffness. On the other hand, the filled-concrete also increases the column ductility and its resistance against local buckling. The steel shear wall is also recognized as an effective lateral load bearing system that, if properly designed, could present high elastic stiffness, stable hysteretic behavior, high capacity of energy absorption and damping and significant ductility. The thin steel plate buckling is mainly controlled by the ultimate strength of steel. These walls are divided into two types of stiffened and unstiffened. The unstiffened one is convenient in northern America and the post-buckling strength is used there to calculate the bearing capacity of the wall (Hoseinzadeh et al. 2017; Tromposch & Kulak, 1987). There had been several experimental, numerical and analytical researches for investigation of the behavior of concrete filled steel tubes (CFT) columns including (Matsui et al., 1998; Hayashi et al., 1995; Choi et al., 2003; Nakahara et al., 2003; Chung et al., 2007; Zhang et al., 2007; Abed et al., 2013; He et al., 2013; Wang et al., 2017). Primary studies on steel shear walls were started in 1931 by Wagner

* Corresponding author.
E-mail addresses: m.gholami@yu.ac.ir (M. Gholami)

doi: 10.5267/j.esm.2022.2.002

(1931) in which he studied the tensional performance of such components in this system. Afterwards, some other studies were done on post-buckling strength of steel shear wall plate and different theories were developed. Until 1980, limit state design of steel shear wall was established to prevent the out of plane buckling of filling-plates that caused heavy and uneconomical design of stiffener plates. In more recent years some studies such as (Deylami et al., 2000; Berman et al., 2005; Hitaka & Matsui, 2003; Vian, 2005; Astaneh & Zhao, 2002; Kharrazi et al., 2008; Zhang et al., 2011; Hosseinzadeh & Tehranizadeh, 2012; Li et al., 2014) are worthy to be mentioned. Chan et al. (2011) studied decrement of stiffness and resistance by means of non-linear, finite elements method in a single span frame, with two different thicknesses of steel panel of 5 and 10 millimeters. In this study, the load-displacement method was used and a maximum displacement of 88 mm was applied to the top flange of the top frame beam. The conclusion of this study led to a linear equation for resistance and stiffness decrement. Nie et al. (2013), tested three specimens of steel shear wall without opening and with opening related to a practical case (International Tianjin hotel-China) with a scale of 20% and steel panel thickness of 4 mm. The comparison of experimental and software models based on reverse cyclic loading results and those real results, for stiffness, ductility, and energy absorption of specimens showed higher resistance, good ductility and higher energy absorption. Obviously, these results could be used for opening-included models with lower resistance and stiffness. Hysteresis curves of specimens were compared with those of software results in which the proximity of these two methods is obvious. Also, a simple method for calculation of lateral resistance capacity was presented which was based on the failure mechanism of the shear wall with stiffener by considering the effect of bearing frame and cantilever effect. Wang et al. (2015) studied the seismic behavior of steel shear walls. In order to do this study, nine steel shear wall models were completely analyzed and compared by means of the finite elements method. The results revealed that in order to choose a proper form of steel shear wall in severe seismic zones, it is necessary to consider all the possible aspects such as ultimate resistance of the wall, hysteresis behavior, failure modes, ductility and economical aspect. Considering the literature available for the shear walls and CFT columns, it seems obvious that the behavior of these frames has not been studied well on a real scale. Thus, in this study, the behavior of steel shear walls in which the CFT columns are used as vertical boundary elements, is studied using full scale finite elements analyses.

2. Finite elements modeling

Not only the modeling by use of finite elements method creates better means to understand the behavior of CFT column and steel shear wall behavior, but also might be beneficiary in case of lack or loss of experimental results. In this article, the finite elements method is used by means of ABAQUS software, in order to simulate the concrete plastic damage model. This model is available in ABAQUS by default, to simulate the behavior of concrete and other semi-brittle material in many sorts of structures such as beams, trusses, shells and filled objects. This model benefits the concept of isotropic damage in linear range, in combination with isotropic tension and plastic compression to present the non-linear behavior of concrete. Also, it is capable of modeling arbitrary loading conditions for instance, cyclic loading. Decreasing elastic stiffness would also be applied, considering plastic strains in tension and compression. This model is contributed to damaged concrete that is also an integrated model, based on plastic behavior. In this model, the main failure mechanism is related to tensional and compression cracks. Furthermore, the tension and negative one-axial compression response and the stress-strain curve, before the failure point is considered to be linear. The failure point occurs at the same time as the crack starts to propagate in the concrete. After the failure point, the damages become obvious as visible cracks. This is presented as a softened stress-strain curve. When applying one-axial compression, the response is elastic up to the ultimate stress and in the plastic zone, the behavior is mainly presented as stiffened curves and finally, at the ultimate stress point, the behavior is again presented as softened curves.

The stress-strain curve of the concrete is used to forecast its behavior of failure. The curve could be separated into two inclining and declining parts. In this study, a modified model of Kent and Park (1971) was used to define the compressive stress-strain curve of the concrete. A relation of stress-strain is defined for tension in concrete to describe the effects of cracking which belongs to the consequences of tensile stiffening. The equation for modeling in this study was considered to be linear after the cracking of concrete which continues further until the tensile strain is 10 times the cracking strain as stated by Aschheim et al. (2019). Fig. 1 introduces the stress-strain relation of concrete under one-axial tension.

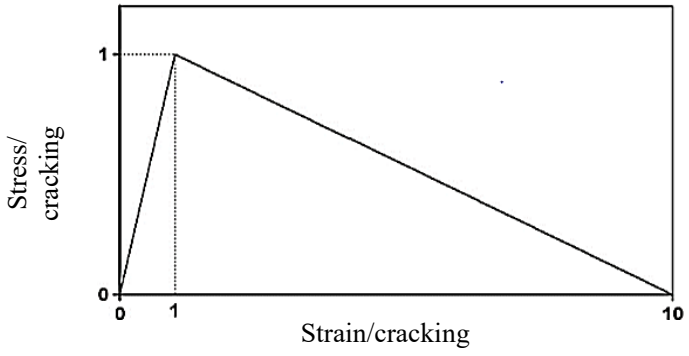

Fig. 1. Stress-strain relation of concrete under tension

Behavior of steel as an elastoplastic material is considered to be similar in tension and compression. For concrete modeling, an eight-node element called Solid C3D8 with 3 degrees of freedom in each node was used. This element type is capable of considering the plastic deformations and cracks in 3 orthogonal directions in each point of integration. In this study non-linear time-dependent behaviors such as creep and shrinkage were not modeled. In order to model the steel plate and steel profiles S4R element was used. the 4-node shell element reduces the number of integration points and reduces the time of numerical analyses. As the cross shear effect has been considered in this element, it could be used in thin or thick-structured models. Also, Tie support is used to model the interaction between concrete and plates of CFT column which considers complete contact between concrete and steel. Furthermore the bond between concrete and steel is considered to be perfect and this will not be detached when the frame deforms.

3. Model verification

To show the capabilities of the model, the experimental results reported by Li et al. (2014) were performed. Li et al. (2014) performed their tests on three two-storey, single-span frames in a large scale with unstiffened steel shear wall and squared CFT columns. The normal concrete-infill box column (NBC) specimen was chosen for verification. The columns in Specimen NCB were infilled by self-consolidating concrete having an expected minimum compressive strength of 28MPa. The effect of using CFT columns as vertical boundary elements of a steel shear wall panel was studied in Li et al. (2014). Material characteristics of the specimen are presented in Tables 1 and 2.

Table 1. Concrete material characteristics of NBC specimen illustrated in Li et al. (2014)

Characteristics	
Concrete strength (MPa)	28
Elasticity modulus (GPa)	26

Table 2. Steel material characteristics of NBC model illustrated in Li et al. (2014)

Characteristics	
Failure strength of shear walls' steel (MPa)	210
Failure strength of beams and columns' steel (MPa)	345
Elasticity modulus (GPa)	200

The comparison of load-drift curves in the NBC test specimen and finite element model is presented in Fig. 2 that shows the good agreement between the experimental results and numerical simulations. Thus, the assumptions used in such modeling procedures can be used for analyzing the real scale models including steel shear wall and CFT columns.

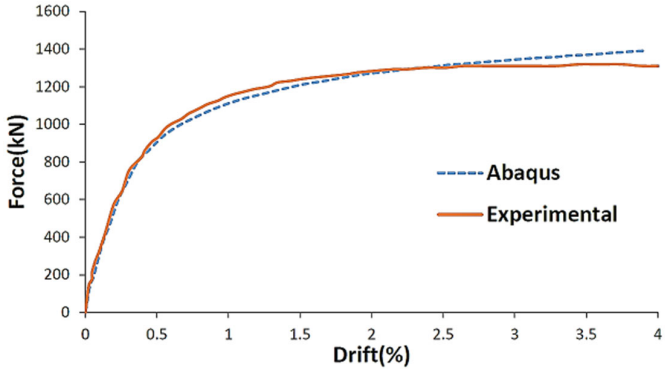

Fig. 2. Comparison between force-drift curves obtained from ABAQUS model with the experimental results of real scale structure.

4. Time history analysis in SAP2000 software

To study and compare the steel shear wall system with bracing system and bending frame system, three ten-storey squared plan structures with 20 meters of plan edge and five equal, 4 meters spans were modeled in SAP2000 software (Fig. 3). Storey heights were equally chosen as 3m. Tables 3 and 4 also present the material properties of the structure and also the details of the elements used in the model. Seven accelerograms were used for non-linear dynamic analysis, in order to use their average output value to control the deformations and internal forces. It has been tried to choose accelerograms, in which the zone structure conforms to the soil type. The accelerograms have a magnitude between 5 and 7 with a far distance from fault and are without any direction effect. To use these accelerograms in non-linear, dynamic analysis, their spectrum must be compatible with the objective earthquake. In this study, the earth is considered to conform code 2800 and to be in a high earthquake risk zone (A=0.3g) which is named as risk-level one. The accelerograms should be scaled before using and the

highest acceleration of each accelerogram is scaled here equal to 1g. After that, the response of the structure is achieved with one degree of freedom using these accelerograms and the response spectrum of the earthquake is then obtained. The spectrum values will then be read between 0.2T and 1.5T. Also, the values of code 2800 will be obtained as an objective spectrum. The ratio of these values will be calculated and the average ratios of these two sets of values will be used as modification factor of that accelerogram. A modified earthquake spectrum for a moment-resisting frame is presented in Fig. 4. The accelerograms and their details are presented in Table 5. Seven earthquakes listed in Table 5 were firstly scaled according to code 2800 for 3 types of soil and high risk zone (A=0.3g) and then they were applied to the model and the displacement of the roof center of mass were determined. All the connections of the beam and columns were considered to be clamped. Connection of steel shear wall to vertical and horizontal boundary elements (beams and columns) were also considered to be joint connections. The loads were uniformly applied to storey floors. Dead load and live load were considered to be 5 and 2kN/m^2. respectively. Also the lateral resisting system is considered to be a moderate steel moment-resisting frame. In two of the models, with X-bracing and steel shear walls, the lateral resistance was only added to four outer frames at the middle span. The steel shear wall was modeled with 13 similar tensile orthogonal strips in SAP2000 software according to the American steel structures design guide. The material used for these strips performs only in tension and does not perform in compression. The shear wall thickness is also considered to be 3mm in all stories.

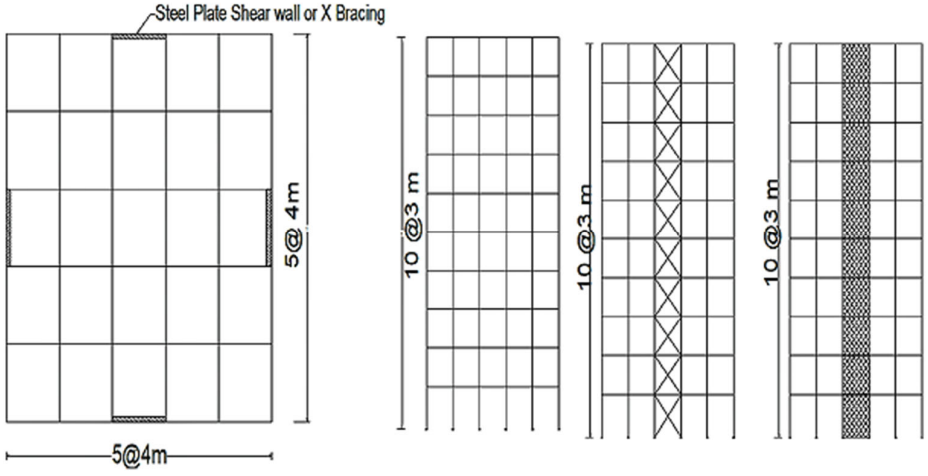

Fig. 3. Plan and facade view of modeled frames in SAP2000 software

Table 3. Material characteristics of modeled structures

Characteristics	
Failure strength of steel (MPa)	240
Ultimate strength of steel (MPa)	370
Elasticity modulus of steel (GPa)	200
28-days strength of concrete (MPa)	25
Elasticity modulus of concrete (GPa)	23

Table 4. Details of modeled frames (beams and columns)

Stories	Beam section	Column section
1 to 4	IPE360	Box360×360×20
5 and 6	IPE330	Box300×300×20
7 and 8	IPE300	Box260×260×16
9 and 10	IPE270	Box260×260×16

Table 5. Details of chosen accelerograms

Record	Station	Date of occurrence	Effective earthquake time (s)	PGA (g)
Bam	Bam	12/26/2003	10	0.775
Tabas	Dayhook	09/16/1978	12	0.4094
Imperial Valley	EL CENTRO ARRAY	05/19/1940	24	0.3128
Loma Prieta	Saratoga - W Valley Coll.	10/18/1989	11	0.3312
Landers	Lucerne	06/28/1992	13	0.788
Manjil	Abbar	06/20/1990	28	0.515
Northridge	ARLETA	01/17/1994	13	0.344

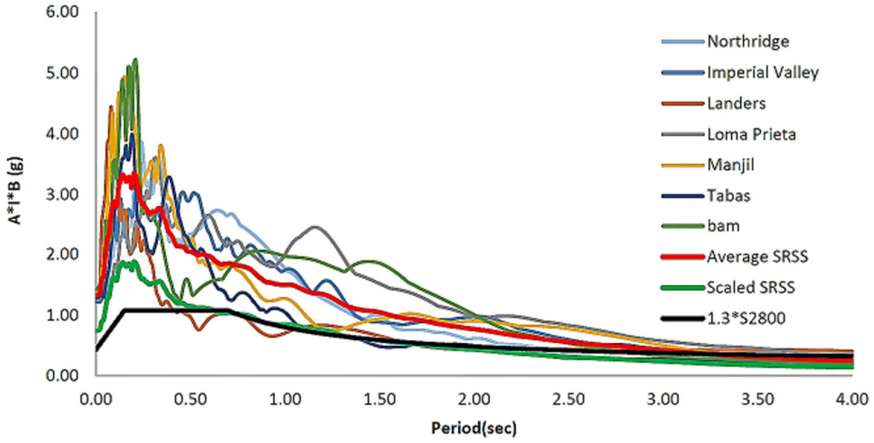

Fig. 4. Scale up of seven accelerograms of previous earthquakes by means of code 2800 standard spectrum

After the non-linear, time-history analysis of the modeled structures, the results of the roof center of mass displacement are presented in Table 6. Also, the displacement graph of the Manjil earthquake is presented in Fig. 5 (as example), that describes the proper performance of steel shear wall.

Table 6. Maximum displacement of roof center of mass

	Displacement of roof center of mass (cm)		
Earthquake	Moment resisting frame	X-bracing	Steel shear wall
Bam	34.7	31.4	31.2
Tabas	24.8	23	23.1
Imperial Valley	24.3	22.9	22.4
Loma Prieta	34.4	26.6	26.3
Landers	26.2	22.4	21.5
Manjil	16.3	11.1	10.5
Northridge	26.5	26.7	26.6

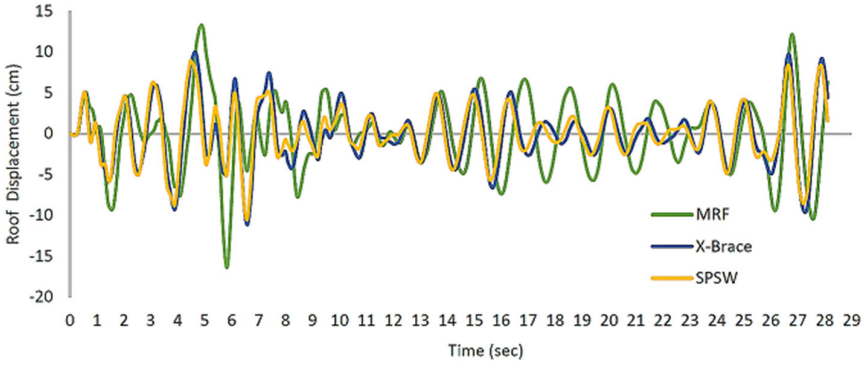

Fig. 5. Displacement of roof center of mass, modeled in SAP2000 after exerting Manjil earthquake for the case of comparison.

By comparing results of maximum displacement of three lateral systems, it is realized that maximum displacement of steel shear wall is 15% lower than the moment resisting frame and 2% lower than X-bracing, which is one of the stiffest steel bracing configurations. A possible reason can be related to the difference between the shape and configuration of steel shear wall and steel X-bracing. Comparison of the stiffness and lateral resistance of these two systems was performed in ABAQUS.

5. Hysteresis and pushover analysis in ABAQUS software

To study more about the seismic behavior of modeled structural systems, hysteresis analysis of first storey from three, one-span frames of modeled structures, was performed in SAP2000. In addition to these three frames, one extra frame is also modeled to study the effect of using CFT columns in an X-bracing frame. The hysteresis analysis was performed for drifts up to 2.5% which had 0.5% increments and two load cycles in each drift value. Hysteresis analysis graphs are presented in Figs. 6 to 9. Due to a hysteresis analysis graph, it is inferred that the energy absorption capacity and steel shear wall system damping is more than moment resisting frame system. But as was previously mentioned, the shear walls consist of 3mm steel panels

while double studs with various sizes have been used for cross over bracing systems. Thus, to study the relative stiffness and resistance of these two systems in the first and tenth floor, a pushover analysis was performed. Having this analysis results, it could be deferred that, 3 mm plate has the same stiffness as 2UNP120 in X-bracing and 8mm plate has the same stiffness and ultimate resistance as 2UNP200 that are presented in Fig. 10. Also Figs. 11 to 14 presents the pushover graphs for different structures and models. As it is obvious from Fig. 10, the linear part of the steel shear wall graph shows a gap that could be related to out of plane buckling of the steel shear wall. After this buckling, while a tensile field is formed in the panel, the secondary stiffness of the frame occurs. Although there is a high stiffness in the cross over bracing frame, the resistance of the frame decreases drastically which is a big deficiency of this system. On the other hand, the steel shear wall shows a proper post-buckling behavior, after the formation of an orthogonal tensile field in which this fault is compensated without any decrement of resistance, as a benefit of this system. As a foresee Ned, although the stiffness of 3mm shear wall is less than the stiffness of cross over bracing frame with 2UNP200 profile, its resistance at 2.5% of drift is so close (with a 8% of difference) to the bracing results, that represents proper post-buckling steel shear wall behavior. After the hysteresis analysis, to study the effect of steel shear wall panel, four single-storey, single-span models with similar beams and columns, consisting of panel thicknesses of 3, 6, 8 and 10mm, were analyzed by pushover method. The results are presented in Fig. 11. Four frames of steel shear wall and cross over bracing systems are also modeled to determine the effect of CFT columns in the frames. Its results are presented in Figs. 12 and 13 that indicate the positive effect of these columns on modeled frames. Of course, the effect of these columns is obvious through all the pushover graphs. This is because of the continuity of shear wall along the column and the way the wall increasingly restrains it.

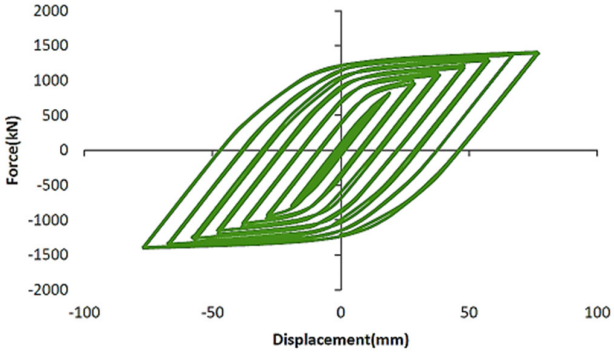

Fig. 6. Hysteresis graph of moment resisting framed structure

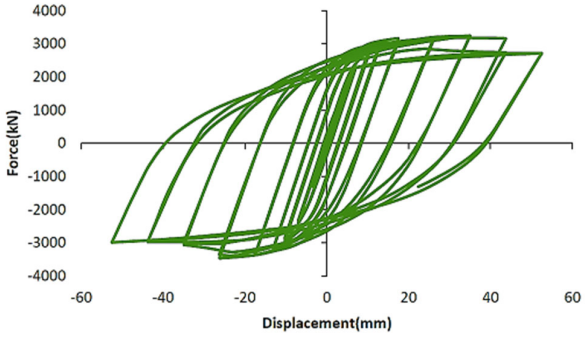

Fig. 7. Hysteresis graph of cross over braced structure

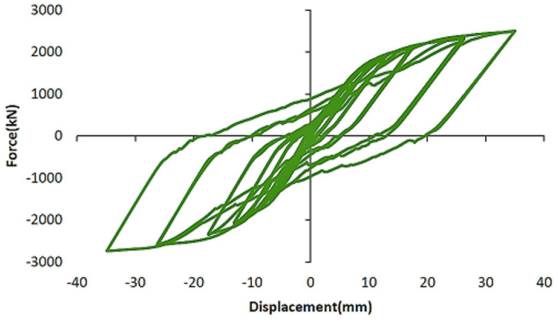

Fig. 8. Hysteresis graph of structure with steel shear wall

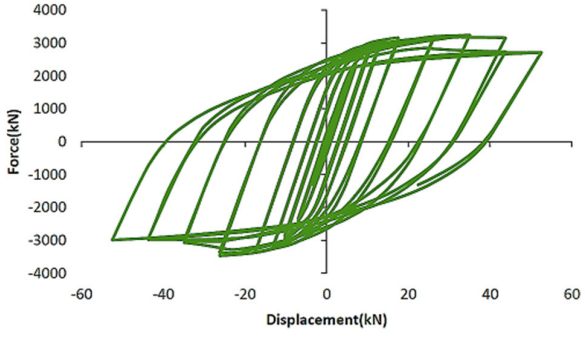

Fig. 9. Hysteresis graph of the structure braced with CFT columns

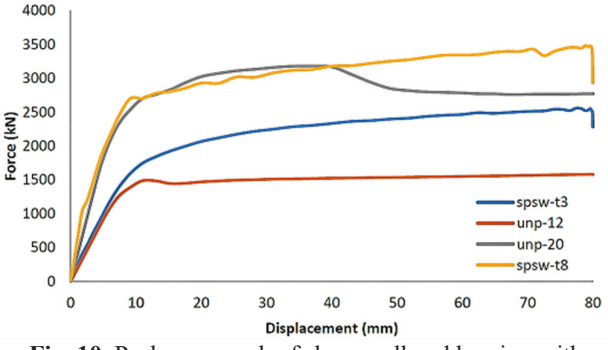

Fig. 10. Pushover graph of shear wall and bracing with 2UNP120 and 2UNP200 profiles

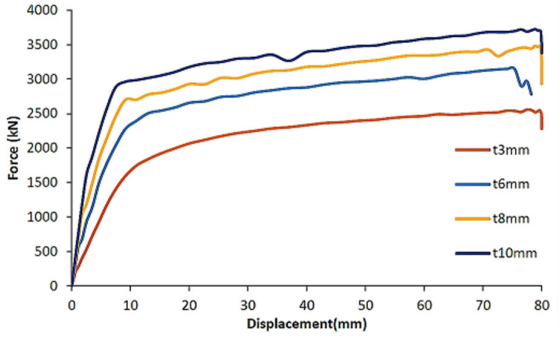

Fig. 11. Pushover graph of steel shear wall with plate thicknesses of 3, 6, 8 and 10 millimeters

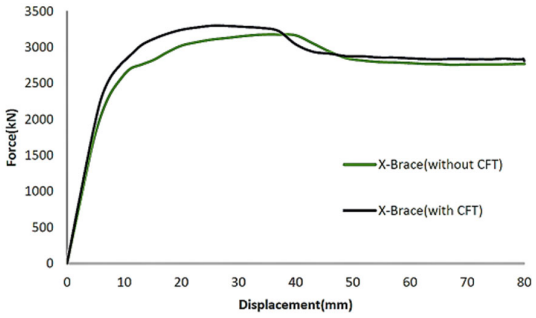

Fig. 12. Pushover graph of cross over bracing, with and without CFT columns

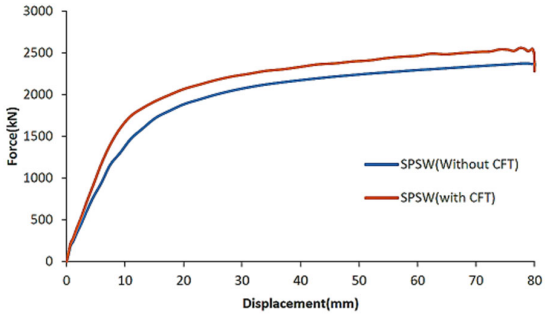

Fig. 13. Pushover graph of steel shear wall, with and without CFT columns

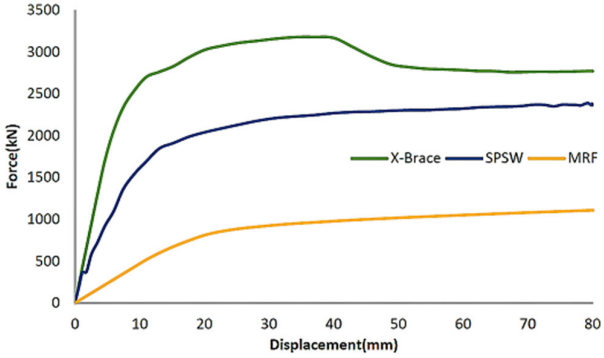

Fig. 14. Pushover graph of steel shear wall, moment resisting frame and cross over bracing in first storey

In Fig. 14, the pushover graph of steel shear wall, moment resisting frame and cross over bracing of a single-storey, single-frame of first storey of a structure are compared. In Fig. 15 pushover graphs of these three systems are compared for the same structure in 10th storey. As was mentioned in Table 4, the sections of beams, columns and bracings for the first storey are IPE360, BOX360×360×20 and 2UNP120, respectively, and for 10th storey these are IPE270, BOX260×260×16 and 2UNP120. From Figs. 14 and 15 it is inferred that in the first storey, the stiffness and resisting of cross over bracing is more than steel shear wall but in 10th storey, as mentioned earlier, the stiffness and resistance of steel shear wall with 3 mm panel is similar to cross over bracing with 2UNP120 profile. In Figs. 16 and 17 the images of frames with cross over bracing and steel shear wall are presented respectively. These images show the ability of ABAQUS software in forecasting failure zones and post-buckling behavior of steel frames.

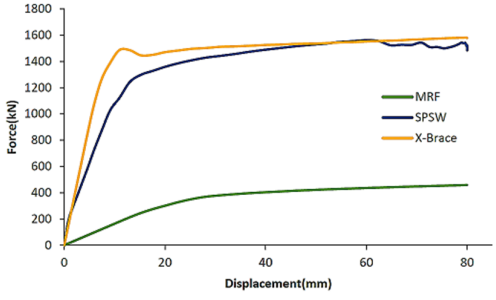

Fig. 15. Pushover graphs of steel shear wall, moment resisting frame and cross over bracing of 10th storey

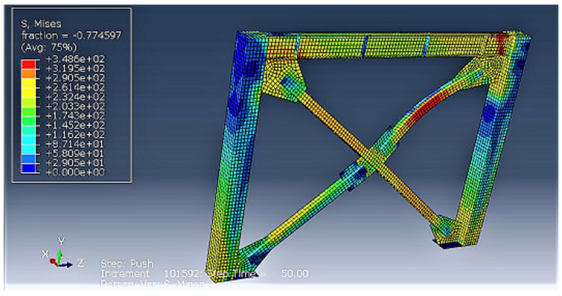

Fig. 16. Cross over bracing frame model of 10th storey and buckling type of compressive bracing

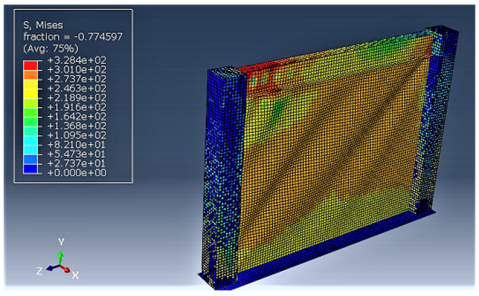

Fig. 17. Steel shear wall model of first storey and the formation of post-buckling tensile field

Table 7 shows the comparison of the strength ratio of the SPSW and the X brace with 2UNP120 and 2UNP200 sections. According to this Table, the highest increase in the ratio of SPSW thickness for 8 mm thickness is 2.19 times and the lowest increase ratio of SPSW for thickness of 3 mm is 1.61 times of UNP12. Similarly, Table 8 compares the strength ratio of steel shear walls with 3, 6, 8 and 10 mm thickness values. According to this Table, the highest increase in the ratio of steel shear wall thickness that is belong to 10 mm thickness is 1.46 times the reference case (i.e. UNP12) and the lowest increase ratio of steel shear wall thickness is 1.24 times the UNP12 case.

Table 7. Comparison of the strength ratio of SPSW and X braces with 2UNP120 and 2UNP200

Modeling mode	The amount of force (kN)	Ratio of force increase
UNP12	1595.61	1
UNP20	3186.08	1.99
SPSW-t3	2575.34	1.61
SPSW-t8	3495.89	2.19

Table 8. Comparison of the strength ratio of SPSW with thicknesses of 3, 6, 8 and 10 mm

Modeling mode	The amount of force (kN)	Ratio of force increase
SPSW-t3	2572.13	1
SPSW-t6	3195.36	1.24
SPSW-t8	3507.52	1.36
SPSW-t10	3758.68	1.46

In addition, Table 9 shows the comparison of the ratio of the increase in the force of the X brace with or without CFT columns. According to Table 9, the maximum gain ratio for the X brace case with the CFT column is 1.04. Table 10 illustrates also a comparison of the strength ratio for SPSW with or without CFT columns. In Table 11, the strength ratio of the three systems (SPSW, the MRF and the X brace) has been compared on the first floor in which the highest and lowest increase in the strength ratio belonged to X brace and SPSW cases, respectively. Similar comparison was made in Table 12 for the strength ratio of the three systems (SPSW, the MRF and the X brace) at the tenth floor.

Table 9. Comparison of the ratio of increase in force of X brace with or without CFT columns

Modeling mode	The amount of force (kN)	Ratio of force increase
X brace (without CFT)	3190.91	1
X brace (with CFT)	3318.18	1.04

Table 10. Compares of SPSW strength ratio with or without CFT columns

Modeling mode	The amount of force (kN)	Ratio of force increase
SPSW (without CFT)	2361.70	1
SPSW (with CFT)	2569.16	1.09

Table 11. Comparison of the strength ratio of MRF SPSW and X brace on the first floor

Modeling mode	The amount of force (kN)	Ratio of force increase
MRF	1122.50	1
SPSW	2403.99	2.14
X brace	3203.83	2.85

Table 12 Comparison of the strength ratio of MRF SPSW and X brace on the tenth floor

Modeling mode	The amount of force (kN)	Ratio of force increase
MRF	461.658	1
SPSW	1571.50	3.40
X brace	1585.49	3.43

Fig. 18 shows the comparison of the maximum force values in different modeling modes. Based on this Figure, the maximum force is related to the 10 mm thick SPSW model and the least force is related to the MRF model.

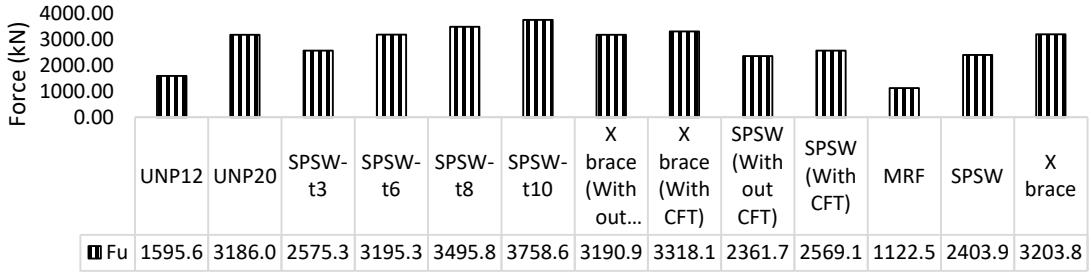

Fig. 18. Comparison of greatest amount of force in different modeling modes.

Fig. 19 also compares the stiffness parameter in different modeling modes in which the highest stiffness is related to the SPSW model with a thickness of 10 mm and the least stiffness is related to the MRF model.

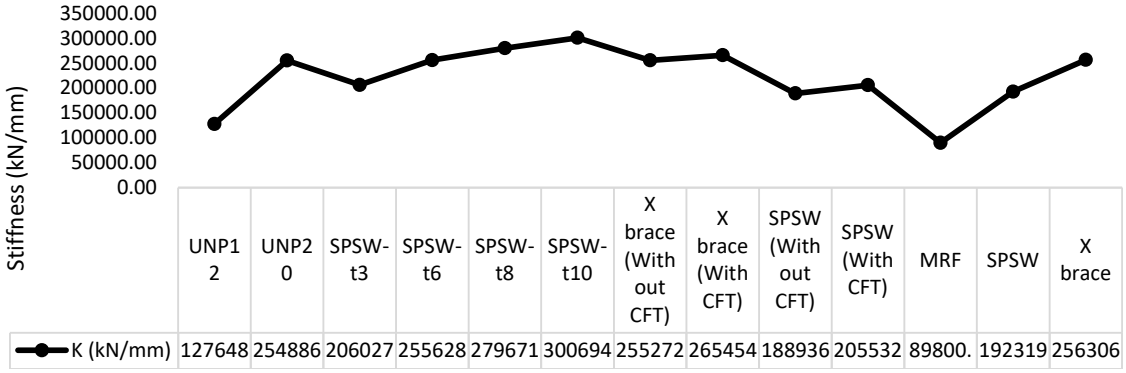

Fig. 19. Comparison of stiffness values in different modeling modes

Fig. 20 presents the variations of the ductility values in different modeling modes that reveals the highest ductility is related to the CFT column X braces model and the lowest ductility is obtained MRF model is used.

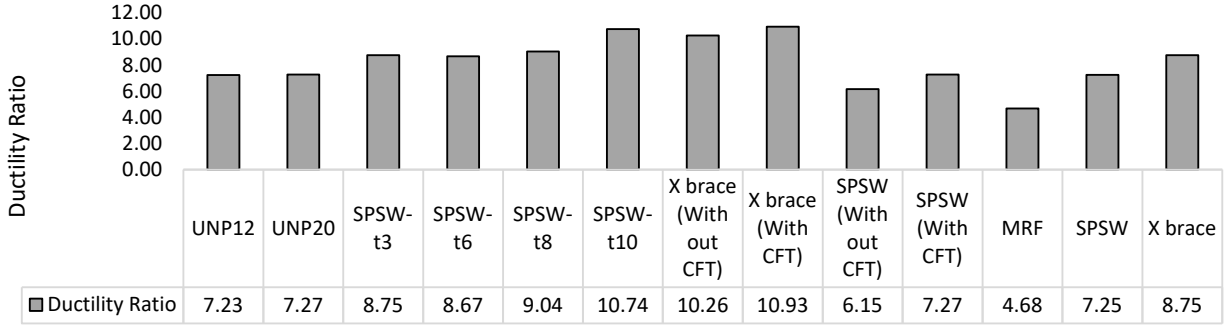

Fig. 20. Comparison of ductility values in different modeling modes

6. Conclusion

By performing the non-linear time-history analysis of structures in SAP2000 software, it was observed that, lowest lateral displacement under seven scaled accelerograms belongs to three systems of steel shear wall, cross over bracing and moment resisting frame respectively. Considering the analysis of the frames in ABAQUS, the effect of CFT columns was studied in steel shear wall and cross over bracing systems and the positive effect of these columns was verified on these two systems. Also, by performing the pushover analysis, the post-buckling behavior of steel shear wall and formation of tensile field was studied. All in all, due to the results of this study, it is deferred that the combination of steel shear wall with CFT columns as boundary elements, is a suitable system to form a high stiffness, ductility and lateral resistance against lateral loads.

References

Abed, F., AlHamaydeh, M., & Abdalla, S. (2013). Experimental and numerical investigations of the compressive behaviour of concrete filled steel tubes (CFSTs). *Journal of Constructional Steel Research, 80*, 429-439.

Aschheim, M., Hernández-Montes, E., & Vamvatsikos, D. (2019). Design of reinforced concrete buildings for seismic performance: practical deterministic and probabilistic approaches. CRC Press.

ASL, M. H., & Safarkhani, M. (2017). Seismic behaviour of steel plate shear wall with reduced boundary beam section. *Thin-Walled Structures, 116*, 169-179.

Astaneh-Asl, A., & Zhao, Q. (2002, April). Cyclic behaviour of steel shear wall systems. In Annual Stability Conference (pp. 18015-3191). Seattle: Structural Stability Research Council.

Berman, J. W., & Bruneau, M. (2005). Experimental investigation of light-gauge steel plate shear walls. *Journal of Structural Engineering, 131*(2), 259-267.

Chan, R., Albermani, F., & Kitipornchai, S. (2011). Stiffness and strength of perforated steel plate shear wall. *Procedia Engineering, 14,* 675-679.

Choi, S. M., Kang, S. B., & Kim, D. J. (2003). Hysteresis performance of CFT columns subjected to low axial force and cyclic lateral loads. *Journal of Korean Society of Steel Construction, 15*(2), 207-217.

Chung, K., Chung, J., & Choi, S. (2007). Prediction of pre-and post-peak behaviour of concrete-filled square steel tube columns under cyclic loads using fiber element method. *Thin-walled structures, 45*(9), 747-758.

Deylami, A., & Daftari, H. (2000). Non-Linear. Behaviour of Steel Plate Shear Wall with Large Rectangular Opening. *In Proceedings of the 12th World Conference on Earthquake Engineering* (pp. 1-7).

HAYASHI, N. (1995). Shear Flexural Behaviour of Concrete-Filled Square Steel Tubular Columns Using High Strength Materials. *In Proceedings of 4th Pacific Structural Steel Conference, Steel-Concrete Composite Structures* (pp. 13-20).

He, W. H., Xiao, Y., Guo, Y. R., & Fan, Y. L. (2013). Pseudo-dynamic testing of hybrid frame with steel beams bolted to CFT columns. *Journal of Constructional Steel Research, 88*, 123-133.

Hitaka, T., & Matsui, C. (2003). Experimental study on steel shear wall with slits. *Journal of Structural Engineering, 129*(5), 586-595.

Hosseinzadeh, S. A. A., & Tehranizadeh, M. (2012). Introduction of stiffened large rectangular openings in steel plate shear walls. *Journal of Constructional Steel Research, 77*, 180-192.

Kent, D. C., & Park, R. (1971). Flexural members with confined concrete. *Journal of the structural division, 97*(7), 1969-1990.

Kharrazi, M. H., Prion, H. G., & Ventura, C. E. (2008). Implementation of M-PFI method in design of steel plate walls. *Journal of Constructional steel research, 64*(4), 465-479.

Li, C. H., Tsai, K. C., Huang, H. Y., Tsai, C. Y., & Lin, C. H. (2014, July). Experimental investigations on steel plate shear walls using box columns with or without infill concrete. *In Proceeding of the 10th National Conference in Earthquake Engineering, Earthquake Engineering Research Institute, Anchorage, AK*.

Matsui, C., Tsuda, K., Kawano, A., & Fujinaga, T. (1998). Structural performance and axial load limit of concrete filled steel circular tubular columns; Concrete juten enkei kokanchu no kozo seino to jukuryoku seigenchi. Nippon Kenchiku Gakkai Kozo-kei Ronbunshu.

Nakahara, H., Ninakawa, T., & Sakino, K. (2003). Cyclic bending behaviour of concrete filled steel tubular columns under constant gravity load. *Journal of Structuctral and Construction Engineering, 568*, 6.

Nie, J. G., Zhu, L., Fan, J. S., & Mo, Y. L. (2013). Lateral resistance capacity of stiffened steel plate shear walls. *Thin-Walled Structures, 67*, 155-167.

Sabelli, R., & Bruneau, M. (2007). Steel plate shear walls (AISC design guide). American Institute of Steel Construction, Inc., Chicago, Illinois.

SAP2000 Version 14.2 [Computer software]. Computer and Structures, Berkeley, CA.

Standard No. 2800, Iranian Code of Practice for Seismic Resistant Design of Buildings, Ministry of Housing and Urban Development of Iran, Tehran, Iran, 4rd edition, 2015.

Tromposch, E. W., & Kulak, G. L. (1987). *Cyclic and static behaviour of thin panel steel plate shear walls*.

Vian, D. (2005). *Steel plate shear walls for seismic design and retrofit of building structures*. State University of New York at Buffalo.

Wagner, H. (1931). Flat sheet metal girders with very thin metal web. Part III: sheet metal girders with spars resistant to bending-the stress in uprights-diagonal tension fields (No. NACA-TM-606).

Wang, M., Yang, W., Shi, Y., & Xu, J. (2015). Seismic behaviours of steel plate shear wall structures with construction details and materials. *Journal of Constructional Steel Research, 107*, 194-210.

Wang, Y. T., CAI, J., & Long, Y. L. (2017). Hysteretic behaviour of square CFT columns with binding bars. *Journal of Constructional Steel Research, 131*, 162-175.

Zhang, J. W., Cao, W. L., Dong, H. Y., & Li, G. (2011). Experimental study on seismic performance of mid-rise composite shear walls with CFT columns and embedded steel plate. *In Advanced Materials Research* (Vol. 163, pp. 2274-2284). Trans Tech Publications Ltd.

Zhang, Y., Xu, C., & Lu, X. (2007). Experimental study of hysteretic behaviour for concrete-filled square thin-walled steel tubular columns. *Journal of Constructional Steel Research, 63*(3), 317-325.